JOURNAL OF GEOPHYSICAL RESEARCH, VOL. 112, D18111, doi:10.1029/2007JD008685, 2007

Observations of fine-scale transport structure in the upper troposphere from the High-performance Instrumented Airborne Platform for Environmental Research

Kenneth P. Bowman,[1] Laura L. Pan,[2] Teresa Campos,[2] and Rushan Gao[3]

Received 21 March 2007; revised 15 June 2007; accepted 11 July 2007; published 26 September 2007.

[1] The Progressive Science Mission in December 2005 was the first research use of the new NCAR High-performance Instrumented Airborne Platform for Environmental Research (HIAPER) aircraft. The Stratosphere-Troposphere Analyses of Regional Transport (START) component of the mission was designed to investigate the dynamical and chemical structure of the upper troposphere and lower stratosphere. Flight 5 of the Progressive Science mission was a START flight that sampled near the tropopause in an area between the main jet stream and a large, quasi-stationary, cutoff low. The large-scale flow in this region was characterized by a hyperbolic (saddle) point. In this study the in situ measurements by HIAPER are combined with flow analyses and satellite data to investigate the quasi-isentropic stirring of trace species in the upper troposphere. As expected from theoretical considerations, strong stretching and folding deformation of the flow near the hyperbolic point resulted in rapid filamentation of air masses and sharp gradients of constituents. Calculations of the stirring using operational meteorological analyses from the NCEP Global Forecast System model produced excellent agreement with HIAPER and satellite observations of trace species. Back trajectories indicate that elevated ozone levels in some filaments likely came from a large stratospheric intrusion that occurred upstream in the jet over the north Pacific Ocean. The methods presented here can be used with operational forecasts for future flight planning.

Citation: Bowman, K. P., L. L. Pan, T. Campos, and R. Gao (2007), Observations of fine-scale transport structure in the upper troposphere from the High-performance Instrumented Airborne Platform for Environmental Research, *J. Geophys. Res.*, *112*, D18111, doi:10.1029/2007JD008685.

1. Introduction

[2] The High-performance Instrumented Airborne Platform for Environmental Research (HIAPER) Gulfstream V research aircraft was delivered to NCAR in March 2005. The Progressive Science Mission was designed to develop experience with the flight characteristics of the new aircraft and to carry out preliminary testing of the instrumentation. Initially intended to take place throughout the autumn of 2005, various issues led to the mission being compressed into the period between 22 November 2005 and 23 December 2005. The Progressive Science Mission consisted of five distinct projects with diverse scientific goals and flight requirements, ranging from low-altitude studies of Pacific marine stratus clouds to high-altitude dropsonde testing. The data described here are from flight 5 of the Progressive Science Mission, which took place on 9 December 2005. This flight was part of the Stratosphere-Troposphere Analyses of Regional Transport (START) component [*Pan et al.*, 2007]. The goals of the START project are to characterize the dynamical and chemical structure of the upper troposphere and lower stratosphere (UT/LS) region. Specifically, to understand the chemical transition between the troposphere and stratosphere, to characterize stratosphere-troposphere exchange and stirring; and to investigate the role of large- versus small-scale dynamical processes in controlling the chemical composition of the UT/LS. Results from other START flights are described elsewhere [*Pan et al.*, 2007; *Young et al.*, 2007].

[3] Flight 5 of the Progressive Science Mission was a START flight designed to measure trace constituents and dynamical variables in the area around a saddle or hyperbolic point in the large-scale flow, in this instance associated with a large cutoff low off the west coast of North America. This was chosen as one type of flow pattern that has a major impact on trace constituent distributions through transport and stirring in the UT/LS region. Because the wind velocity vanishes at the hyperbolic point, it is also referred to as a stagnation point. (See, for example, *Ottino* [1989] or *Wiggins*

[1]Department of Atmospheric Sciences, Texas A&M University, College Station, Texas, USA.
[2]National Center for Atmospheric Research, Boulder, Colorado, USA.
[3]Chemical Sciences Division, Earth System Research Laboratory, NOAA, Boulder, Colorado, USA.

0148-0227/07/2007JD008685$09.00

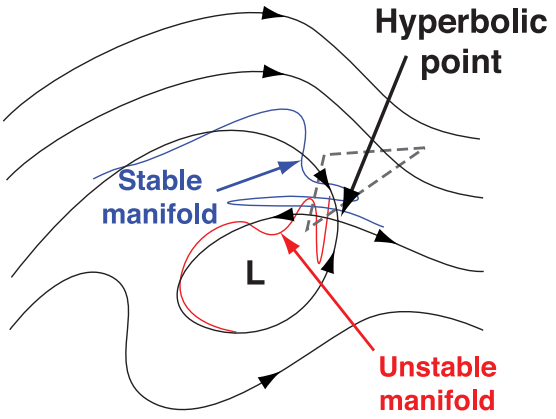

Figure 1. Schematic of the instantaneous streamlines and hyperbolic or saddle point near a cutoff low. Arrows indicate the direction of flow along the streamlines. The blue and red curves represent the stable and unstable manifolds associated with the hyperbolic point, respectively. Time dependence of the flow field causes strong folding and stretching of the fluid near the hyperbolic point. The dashed gray line is the approximate flight track taken by the HIAPER aircraft relative to the hyperbolic point.

[1992] for a discussion of possible two-dimensional flow geometries.) Previous observational and diagnostic studies of atmospheric flows have examined similar features [e.g., *Appenzeller and Davies*, 1992; *Appenzeller et al.*, 1996; *Beuermann et al.*, 2002].

[4] An idealized picture of the upper tropospheric flow is shown in Figure 1, and details of the synoptic evolution of the flow are discussed in section 4.2. The location of the cutoff low is marked by the L. We treat the flow as being approximately two dimensional (i.e., approximately isentropic). The black lines are instantaneous streamlines of the flow. In the hypothetical case where the flow is steady (not time-dependent), particle trajectories follow the streamlines. In that case there are two special sets of particles that lie along the streamlines that intersect at the hyperbolic point. The stable trajectories converge into the hyperbolic point with time, while the unstable trajectories diverge away from the hyperbolic point. These sets of points form surfaces in space and time that are referred to as manifolds in the dynamical system literature. In the steady case these manifolds would strictly divide the interior of the low from the exterior.

[5] In the atmosphere, of course, the flow is not steady, but varies with time. During the interval when the saddle structure and hyperbolic point exist, however, there will also exists sets of particles that converge into and diverge from the hyperbolic point, that is stable and unstable manifolds [*Haller and Poje*, 1998]. Because of the time dependence of the flow, however, the manifolds, and the fluid itself, tend to be folded and stretched near the hyperbolic point into curves like those shown in red and blue in Figure 1 [*Ottino*, 1989; *Wiggins*, 1992; *Miller et al.*, 1997; *Rogerson et al.*, 1999; *Yuan et al.*, 2002, 2004]. This stretching and folding near hyperbolic points is the primary process responsible for large-scale isentropic stirring in the atmosphere. By bringing together fluid from different locations, the stretching and folding can produce large local gradients in trace species, eventually leading to mixing at the molecular level. Note that hyperbolic points do not exist only around cutoff lows and highs, although they are generally easier to visualize near such slow-moving cutoff features.

[6] In this study we analyze trace species distributions near the hyperbolic point using satellite data and observations from HIAPER and compare the results with a kinematic analysis of the flow that maps the locations of the manifolds. The dashed line in Figure 1 shows the approximate flight track of the aircraft relative to the low and the hyperbolic point. HIAPER flew two transects across one of the unstable manifolds that diverge from the hyperbolic point. We show that operational meteorological analyses capture the stirring process near the hyperbolic point very well.

2. Data

2.1. In Situ Data

[7] A comprehensive suite of instruments is under development for HIAPER. At the time of the Progressive Science Mission, however, the available instrumentation consisted of basic meteorological sensors (temperature, pressure, position, and winds), which were undergoing calibration and testing, and instruments to measure water vapor, carbon monoxide, and ozone. Ozone (O_3) was measured by a NOAA Earth System Research Laboratory dual-beam UV-absorption ozone photometer which has an overall uncertainty of 5% [*Proffitt and McLaughlin*, 1983]. Time resolution of the O_3 instrument was about 2–3 s for the HIAPER configuration.

[8] In situ water vapor concentrations were measured on the G-V using a MayComm Open-Path Laser Hygrometer (OPLH) sensor. This inlet-free, dual-channel instrument detects optical absorption of water vapor at 1.37 um. Conversion from concentration/number density to mixing ratio units are achieved using fuselage mounted static pressure and air temperature sensors. Water vapor is measured with an estimated accuracy of 5–10% at a time resolution of 20 Hz which were averaged to 1 s intervals for this analysis. The sensor was designed with two optical paths, 10 cm and 130 cm, to allow quantification in both high- and low-humidity environments. Information from the two channels are combined to report a single water vapor mixing ratio that is valid over a range from 1 to 30,000 ppmv. The limiting factor in assigning uncertainty is the 5% calibration system uncertainty. Comparison between the laser hygrometer and chilled mirror sensors showed good agreement over the overlapping performance range.

[9] Meteorological parameters and trace gas measurements from the mission were calibrated and archived by the NCAR Research Aviation Facility.

2.2. Other Data

[10] In addition to the in situ data collected by HIAPER, this study makes use of large-scale assimilated meteorological products from the NOAA National Centers for Environmental Prediction (NCEP) operational Global Forecast System (GFS) model. These data consist of global grids of temperature, geopotential height, humidity, three-dimensional winds (u, v, ω), vorticity, and tropopause pressure with $1^\circ \times 1^\circ$

longitude-latitude resolution and 26 standard pressure levels. GFS forecasts were used for some aspects of flight planning, and the 6-hourly analyses were archived for later use.

[11] We also use imagery from the water vapor channel of the NOAA GOES-10 satellite. GOES images were obtained from the NOAA Comprehensive Large Array-data Stewardship System (CLASS).

3. Methods

[12] The motion of air masses and the kinematic structure of the atmospheric flow is investigated by computing three-dimensional trajectories of hypothetical massless air parcels (referred to here as particles) using the GFS winds and the TRAJ3D trajectory model of *Bowman* [1993]. The air parcel trajectories are the solution to the equation

$$\frac{d\mathbf{x}}{dt} = \mathbf{v}(\mathbf{x}, t), \qquad \mathbf{x}(t_0) = \mathbf{x_0}, \tag{1}$$

where $\mathbf{x}(t)$ is the three-dimensional particle position at time t and $\mathbf{v}(\mathbf{x}, t)$ is the velocity as a function of position and time. The velocity $\mathbf{v}$ is the large-scale (resolved) three-dimensional velocity from the GFS analysis. Vertical motion is computed in pressure coordinates using the vertical velocity ω. Equation (1) is solved numerically with the TRAJ3D model, which uses a standard fourth-order Runge-Kutta scheme with, in this case, 32 time steps per day. Velocities at arbitrary $\mathbf{x}$ and t are computed by linear interpolation in space and time. Details are given by *Bowman* [1993] and *Bowman and Carrie* [2002].

[13] To produce maps of the stable and unstable manifolds we use a numerical approach to estimate the stretching deformation the fluid undergoes following the motion [*Haller*, 2000; *Winkler*, 2001]. To create a snapshot of the stable and unstable trajectories at reference time t_0, a dense grid of particles is initialized at t_0 covering the area of interest. In this case the grid is 1024 $\times$ 512 particles initialized on the 320 K potential temperature surface. An isentropic surface is used only for convenience, and the results are essentially identical if the parcels are initialized on the 300 hPa surface. The results are not sensitive to increasing the grid resolution.

[14] The particle locations are integrated backward and forward in time to $t_0 - \delta t$ and $t_0 + \delta t$. The resulting trajectories are used to calculate how quickly particles that are initially adjacent separate from each other. Particles that lie near each other, but on opposite sides of a stable manifold, separate quickly as time increases because their motion tends to carry them apart along the two diverging unstable manifolds. Particles that are on the same side of the stable manifold, however, separate relatively slowly, as they tend to move in the same direction along one or the other unstable manifold. The separation at $t_0 + \delta t$ is computed for each neighboring pair of particles, and plotted at their initial locations using blue coloring. The more rapidly the particles separate, the more saturated the color. In a similar manner, backward in time calculations are used to find the unstable manifolds, which are plotted in red. The colors match the red and blue curves representing the unstable and stable manifolds in Figure 1. The time-integration parameter δt is found through numerical experiments. The calculations show that after about one day the picture sharpens rapidly, then becomes increasingly complex as more and more of the structure of the stable and unstable trajectories is mapped out. A value of δt = 3 days is sufficient to map out the principal structure of the flow near the hyperbolic point.

4. Results

4.1. Synoptic Evolution

[15] The flight track for flight 5 was designed to sample the region around the hyperbolic point. Figure 2, which contains a sequence of 6 once-daily (1945 UTC) GOES water vapor images, illustrates the evolution of the synoptic situation associated with the cutoff low and hyperbolic point. Superimposed on the GOES images is the geopotential height of the 300 hPa surface. The flight track is plotted in Figure 2d from 9 December 2005, which coincides with the aircraft flight. The short flight segment shown is magenta is the part of the flight track within ±15 min of the GOES image time. As is typical for a vertical sounding instrument, the weighting function for the GOES water vapor channel is relatively broad and has a peak between about 400 and 500 hPa.

[16] During the time period surrounding the flight, the jet stream in this region is dominated by a large, nearly stationary ridge located near the west coast of North America. The development of the cutoff low can be traced back to a trough that is visible on 6 December 2005 (or even earlier), indicated by heavy dashed lines in Figures 2a and 2b. By 7 December 2005 (Figure 2b) the trough has moved around the top of the ridge, and several mesoscale cyclones, visible in the water vapor data in Figure 2b, have moved into the trough. By 8 December 2005 (Figure 2c) the trough has become a cutoff low, which persists through the remaining panels. As will be shown later, there is a hyperbolic point in the flow even before the trough develops into a cutoff low. Between 11 December 2005 and 14 December 2005 (not shown) the low finally weakens and moves off to the east.

[17] A prominent feature in the GOES water vapor image at the time of the flight is a very dry filament of air, labeled as such in Figure 2d that is oriented approximately west-to-east across the aircraft flight track. The back trajectory analysis, discussed in section 4.4, indicates that the dry air came from the north side of the hyperbolic point. As it approached the hyperbolic point, the flow stretched the dry air into the long narrow feature seen in the satellite images.

4.2. Flight Track

[18] Figure 3 shows the flight track for flight 5 and the geopotential height of the 300 hPa surface at 1800 UTC on 9 December 2005. The aircraft took off at approximately 1815 UTC on 9 December 2005 from Jefferson County Airport near Boulder, Colorado and flew two nearly identical counterclockwise circuits around a roughly triangular path. The aircraft then descended and returned to the departure airport at approximately 0100 UTC on 10 December 2005. At the time of the flight, there was a low in eastern Colorado and a large cutoff low off the coast of Southern California.

[19] Cross sections of the flight track and several atmospheric variables, projected on the line A–A′, are shown in Figures 4 and 5. The in situ ozone concentration measured

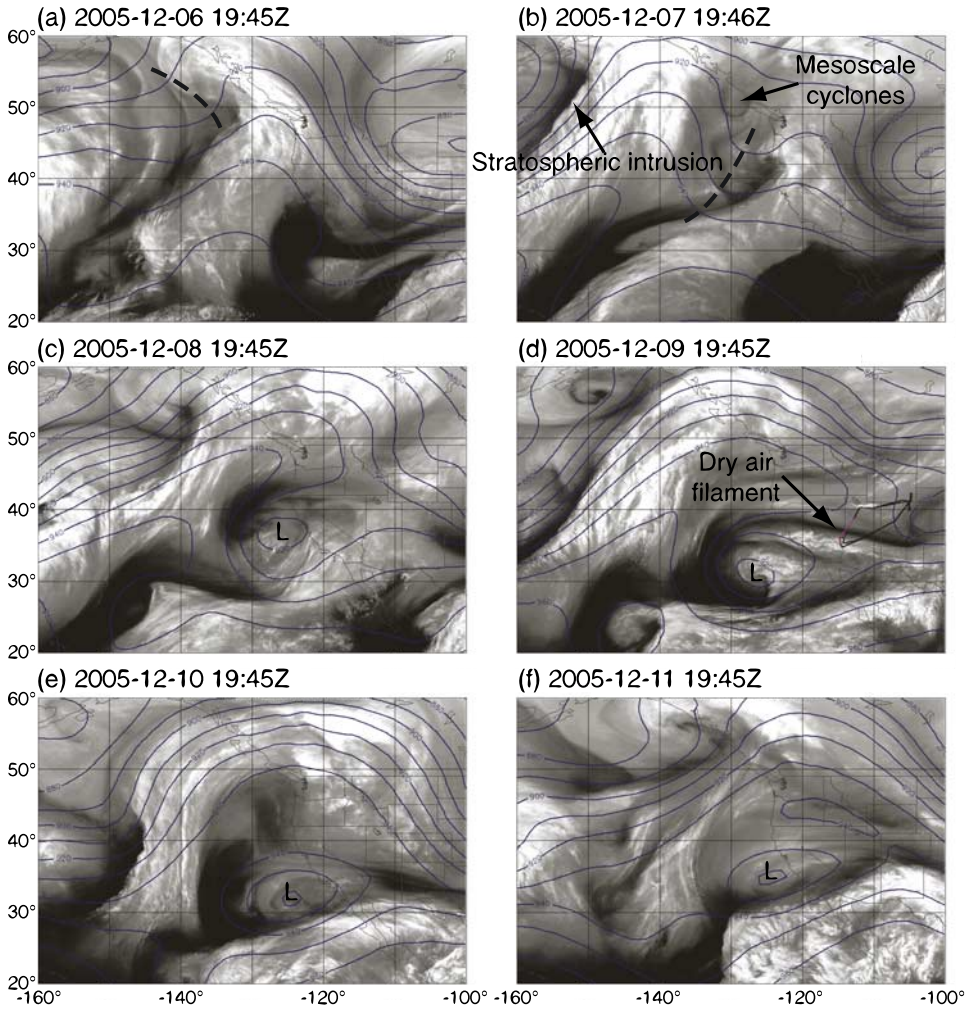

Figure 2. (a–f) GOES water vapor imagery and 300 hPa geopotential height (dm) at 24-hour intervals. The aircraft flight took place on 9 and 10 December. The aircraft flight track is plotted in Figure 2d. A 30-min segment of the flight track centered on the GOES image time is highlighted in magenta.

by the aircraft is color-coded on the flight track in Figure 4, while water vapor mixing ratio is shown in Figure 5. Gray indicates missing data. In Figure 4 arrows indicate the flight direction for selected legs. Also shown are the potential temperature (black), potential vorticity (purple), GFS analyzed tropopause pressure (orange), and the wind component normal to the cross section (gray), all taken from the 1800 UTC GFS analysis on 9 December 2005. For clarity the wind contours are omitted from Figure 5.

[20] The aircraft encountered a stratospheric intrusion associated with the low over eastern Colorado on the initial ascent. This can be seen as the small region of high ozone (red, Figure 4), low water vapor (red, Figure 5), and high PV (purple contours) between about 500 and 600 hPa. By the time of the final descent and landing, the low had moved farther east. The flight track did not intersect the intrusion on the descent leg, and high ozone and PV are not seen in the aircraft observations. During the first circuit, near 300 hPa, the aircraft encountered a region of dry air, labeled as such in Figure 5. Elevated ozone is also present in this region, which is shown in greater detail in section 4.3.

[21] The first circuit around the path was carried out at nearly constant pressure (~300 hPa) and was completed at approximately 2130 UTC, at which time the aircraft ascended to near 250 hPa and flew the second circuit. During this circuit several vertical profiles were carried out, three into the lower stratosphere (indicated by high ozone and low water vapor in yellow) and one descent to about 400 hPa.

[22] This study is primarily concerned with the horizontal variations in trace constituents produced by the large-scale flow. Therefore we focus on the first circuit, carried out near 300 hPa. The flight track carried the aircraft very near a hyperbolic point in the flow located near the point labeled B in Figure 3. In this region the aircraft encountered wind speeds as low as 1 m s^{-1} at 300 hPa.

4.3. In Situ Observations

[23] In order to better locate the aircraft trace species measurements in relation to the atmospheric flow pattern, the water vapor and ozone concentrations along the flight track are shown in Figures 6 and 7. In Figures 6 and 7, the

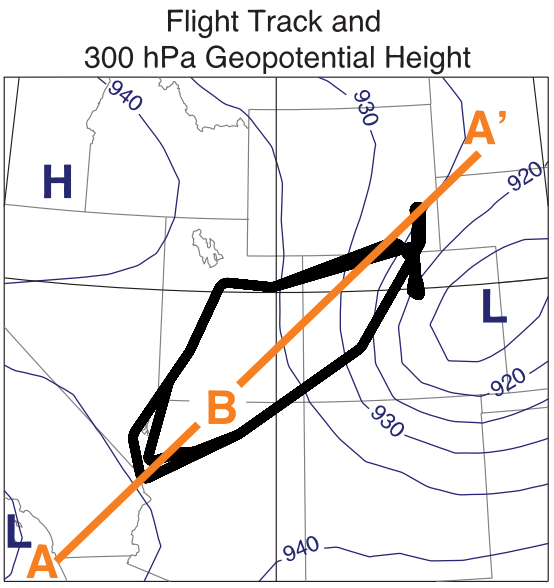

Figure 3. Detail map showing the flight track for Progressive Science flight 5. Contours are the height of the 300 hPa pressure surface in dm at 1800 UTC on 9 December 2005. An atmospheric cross section along the line A–A′ is shown in Figure 4. The flow around the 300 hPa level has a saddle point or stagnation point near the label B.

trace species concentration is plotted in the third dimension above the aircraft track, which is shown in black atop the GOES water vapor imagery. The horizontal axes are longitude and latitude, rotated so that the view is from slightly north of west, looking eastward along the dry air filament seen in Figure 2d. The vertical coordinate is the concentration of the species of interest. The dry air filament in the GOES image corresponds very closely to the minimum water vapor values measured by HIAPER. Minimum values are near 100 ppmv. Sharp horizontal gradients of water are seen on either side of the filament, with water vapor amounts changing by about a factor of three within 0.5 degrees (~50 km).

[24] Figure 7 is similar to Figure 6, but shows the in situ ozone concentration measured by HIAPER. This view reveals that the dry air filament is coincident with a very narrow filament of high-ozone air that shows up as spikes (labeled spike 1 and spike 2) on the outbound and return legs where they cross the dry air filament. Peak ozone values in the spikes are 60–70 ppmv. This is well below stratospheric values, but well above normal free tropospheric values.

[25] To confirm the hypothesis that the GOES water vapor and in situ aircraft data are produced by the type of transport and flow deformation sketched in Figure 1, we analyze the transport characteristics of the flow, including backward and forward trajectories for air parcels sampled along the aircraft flight track.

4.4. Flow Analysis

[26] We begin an analysis of the flow in the region around the hyperbolic point by examining the trajectories of air parcels sampled by the HIAPER aircraft. For clarity, we focus on a segment of the flight track that crosses the dry air filament and ozone spikes seen in Figures 6 and 7. The segment is labeled "Outbound leg" in Figure 6. In situ

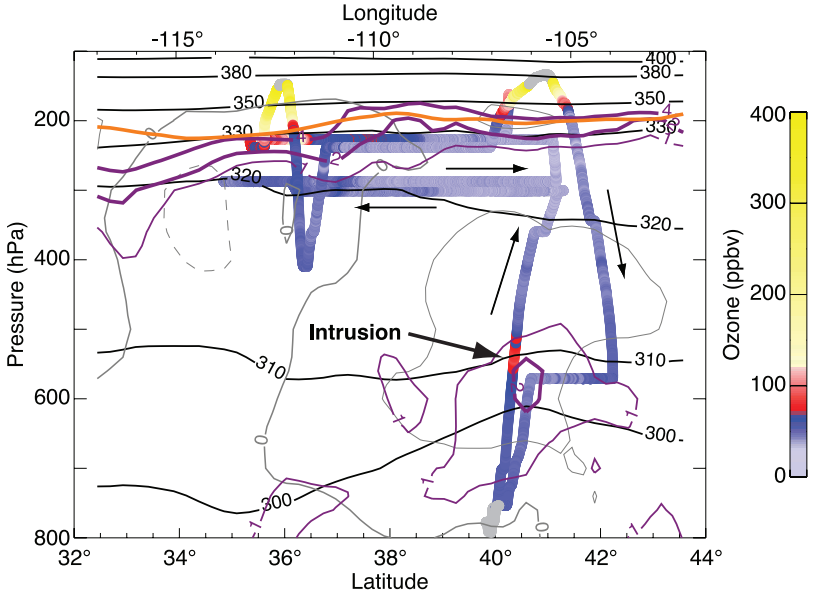

Figure 4. Atmospheric cross section along the line A–A′ in Figure 3. The aircraft flight track projected onto the plane of the cross section is shown with in situ ozone concentration color coded. Gray indicates missing data. The flight was from approximately 9 December 2005, 1815 UTC, to 10 December 2005, 0100 UTC. Variables in the cross section are taken from the 9 December 2005, 1800 UTC, GFS analysis and so are not representative of the later portions of the flight. The potential temperature is plotted in black (K); the potential vorticity is plotted in purple (pvu), the GFS WMO tropopause is plotted in orange, and the wind component normal to the cross section is plotted in gray (m s^{-1}). The wind contour interval is 10 m s^{-1}. Winds are weak in this region. Arrows indicate the flight direction for selected legs.

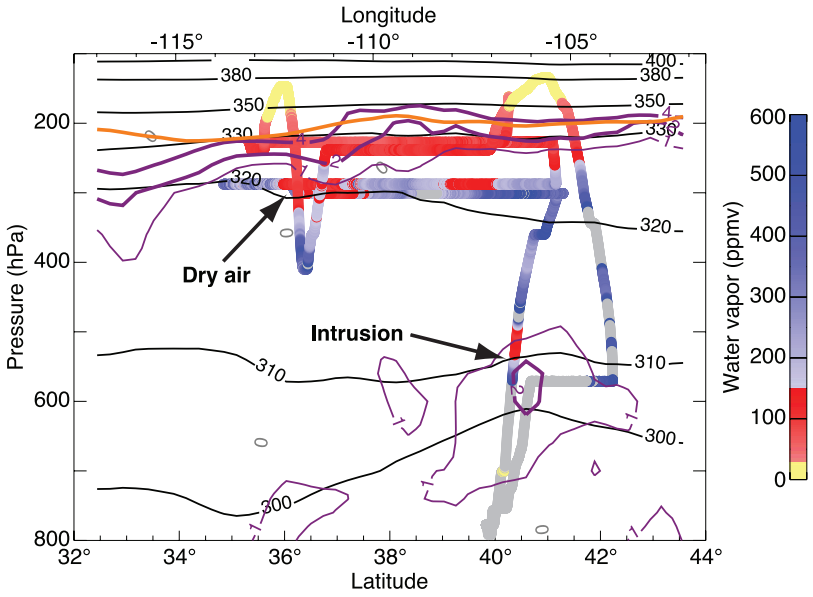

Figure 5. As in Figure 4 for in situ water vapor concentration. Wind speed is omitted.

measurements of ozone and water vapor from HIAPER for this flight segment are shown in Figure 8 at 1-s time resolution. The ozone spike to ~65 ppbv and the water vapor minimum occur near 1945 UTC. The colored dots are points along the flight track at 1-min intervals for which trajectories are calculated. At the typical aircraft flight speed, these locations are separated by ~15 km along the ground track. Forward and backward trajectories for the aircraft locations at the time of each dot are computed and combined into a single path.

[27] The trajectories are plotted in Figure 9, color coded to match the dots in Figure 8. The parcels in the ozone spike are colored red, those to the north of the spike along the flight track are colored green, and those to the south are blue. All of the trajectories converge on the flight track segment and then move generally counterclockwise around the cutoff low. Before the flow brought the particles together near the hyperbolic point, however, they followed very different trajectories. With one exception, parcels colored blue came from the subtropics near 20°N between

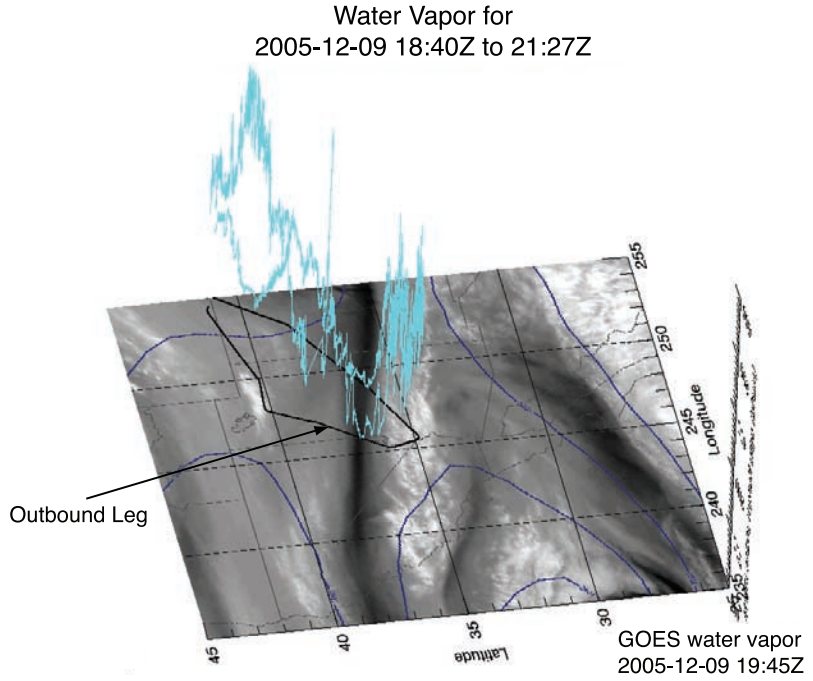

Figure 6. GOES water vapor imagery and in situ water vapor concentration from HIAPER (cyan). The vertical axis is HIAPER water vapor concentration, plotted with a scale ranging from 100 to 600 ppmv. The view is from slightly north of west, looking eastward along the dry air filament seen in Figure 2d.

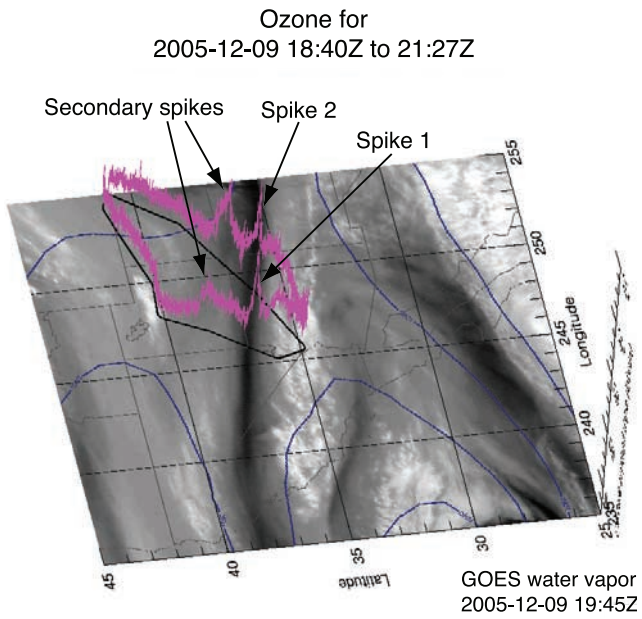

Figure 7. GOES water vapor imagery and in situ ozone concentration from HIAPER (magenta). The vertical axis is HIAPER ozone concentration, plotted with a scale ranging from 30 to 120 ppbv. View as in Figure 6.

about 300 and 400 hPa. The red and green parcels were recently at high latitudes and lower pressures (250 to 300 hPa). The red parcels were at higher altitudes than the green parcels during the recent part of the trajectory, but the highest ozone value (from the center of spike 1) is associated with the red parcel that ascended from near 500 hPa at 160°W. The back trajectories in Figure 9 (bottom) look very similar in isentropic coordinates. Two days before the aircraft observations, the red parcels lie at potential temperatures from 322 to 325 K, while the green parcels are slightly lower, between 319 and 322 K.

[28] The high-ozone air in the two spikes can be attributed to two possible sources. One possibility is that the air passed very near to the tropopause, as estimated in the GFS analysis, within about 2 days of the aircraft observation. This can be seen in Figure 9 (bottom). During this residence at the top of the troposphere, high-ozone air from the stratosphere could have been mixed into the upper troposphere by small-scale turbulence. Several facts weigh against this possibility, however. First, in the time preceding the aircraft observations, the three parcels colored red followed similar paths near the tropopause, but only one had high ozone, and that parcel was not the one that passed closest to the tropopause. Second, the ozone spikes encountered on the outbound and return legs are very similar, suggesting a large coherent ozone anomaly that is hard to explain by small-scale mixing.

[29] Another possibility is that the high-ozone air is the result of a previous stratospheric intrusion that has been stretched into a narrow filament by the flow near the hyperbolic point. We check this hypothesis by analyzing the back trajectories of the air parcels that are in and near the ozone spikes. Two days earlier, at 1800 UTC on 7 December 2005, the red and green particles were located over the Pacific Ocean on the western side of the large ridge. At this time a large stratospheric intrusion was located between 150 and 160°W near 50°N. The intrusion can be seen as a patch of dry air in Figure 2b. This intrusion, as defined by the 2 pvu surface, reached down to about 500 hPa. At this time the air parcels that were later sampled by HIAPER were located very close to this intrusion, as can be seen in Figure 10. The low-ozone green particles passed along the southern flank of the fold, and by all indications did not pick up any stratospheric ozone in the process. The two red particles with relatively low ozone (see Figure 8)

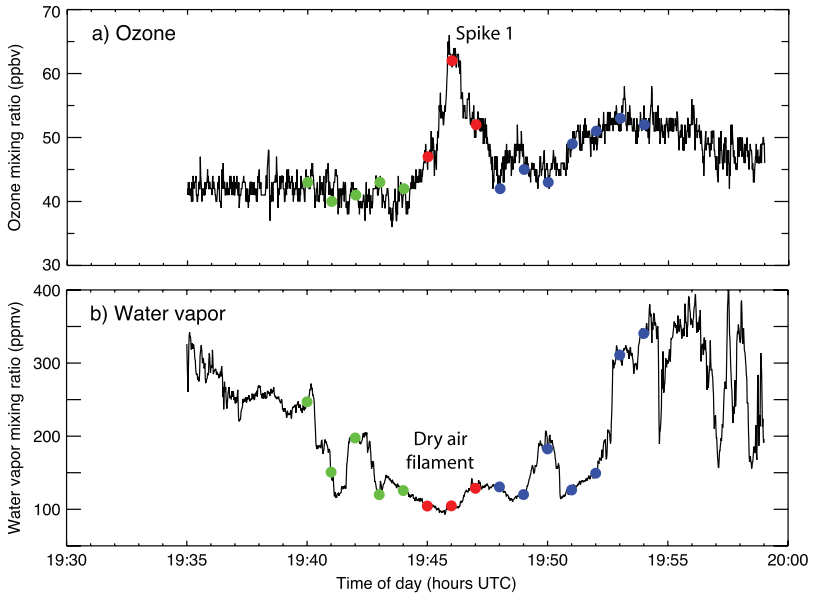

Figure 8. In situ measurements of (a) ozone and (b) water vapor along the flight track segment labeled "Outbound Leg" in Figure 6. The colored dots indicate air parcels for which trajectories are computed using the GFS winds.

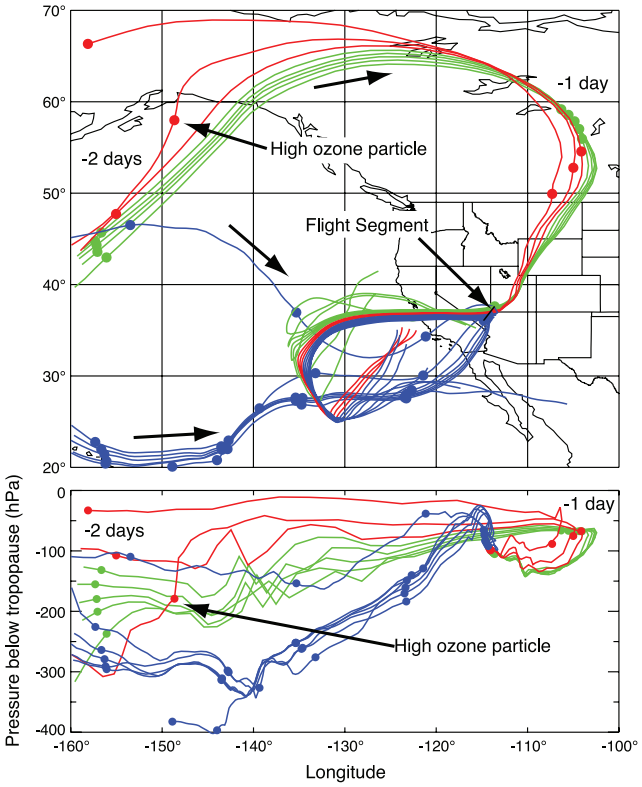

Figure 9. (top) Map and (bottom) longitude-pressure cross section of forward and backward trajectories for air parcels sampled by the HIAPER along a short segment of the flight track. Color codes match the dots in Figure 8. Particle positions are shown at 1800 UTC each day along the backward trajectories. Labels indicate the general position of the red and green particles at −1 day and −2 days. For clarity, only the backward trajectories are shown in Figure 9 (bottom). Arrows indicate the direction of motion of the particles along their trajectories.

passed on either side of the fold, one on the southern side and one on the northern. The particle on the northern side is not visible beneath the 2 pvu surface. The high-ozone particle from the center of the ozone spike (particle labeled "high ozone" in Figure 10) followed a very different trajectory that is much lower than the other red particles. This particle is directly aligned with and slightly downstream of the tropopause fold, suggesting that the high ozone is a result of this stratospheric intrusion that is then stretched by the flow near the hyperbolic point.

[30] To further confirm that the stratospheric intrusion in Figure 10 is the source of the high-ozone air, a forward trajectory calculation is carried out for particles located in the intrusion (Figure 11). Particles are initialized at 0000 UTC on 8 December 2005 in the volume between the 1.5 pvu PV and the 300 hPa pressure surfaces (Figure 11a). This is slightly less than 2 days prior to the aircraft observations. In both panels only the particles that end up close to the aircraft flight level (275 to 325 hPa) at 2100 UTC on 9 December 2005 are shown. The particle positions are integrated forward in time using the TRAJ3D model with GFS winds. The particles move around the top of the ridge and approach the hyperbolic point from the north. As the red air mass in Figure 1 shows schematically, the air from the intrusion ends up straddling the stable trajectory associated with the hyperbolic point. The air from the intrusion on the west side of the stable trajectory is stretched into a narrow filament by the flow near the hyperbolic point, with part of the air mass wrapping up around the cutoff low to the west. The part of the air mass that lies on the east side of the stable trajectory is stretched into a narrow filament extending eastward into Oklahoma and Kansas. Another part of the air mass remains in the main jet stream and is carried eastward beyond the boundaries of the map. There are indications of a second filament forming just to the north of the first that may be associated with the ozone spikes labeled "Secondary spikes" in Figure 7.

4.5. Diagnosis of Hyperbolic Points

[31] The stretching calculations described in section 3 are used to map the stable and unstable manifolds at 9 December 2005 at 1800 UTC. In Figure 12 the stable manifold lies along the closely spaced blue curves that are oriented roughly southwest to northeast through the hyperbolic point. The east–west oriented unstable manifolds are colored red. The trajectory results agree very well with the other data presented here, including the satellite imagery, the aircraft observations, and the forward and backward trajectory analysis for the air parcels sampled by the aircraft. The layering of red and blue manifolds around the boundary of the cutoff low shows the stretching of air masses into long narrow filaments by the flow near the hyperbolic point. This information cannot be obtained by examining streamline maps alone. Related information could be obtained by using reverse-domain filling (RDF) methods; but, in addition to trajectory calculations, RDF requires a global field that can be mapped to the analysis time. The methods used here require only knowledge of the velocity field.

[32] Once a hyperbolic point is located approximately by using the deformation calculation (Figure 12), the manifolds can be calculated quite precisely by using contour advection techniques (not shown). The manifolds calculated in this

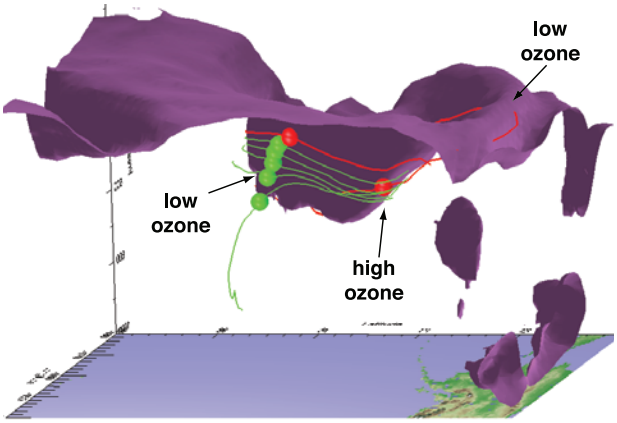

Figure 10. Three-dimensional view of air parcels and trajectories (green and red) and stratospheric intrusion as defined by the PV = 2 isosurface at 1800 UTC on 7 December 2005. The view is looking southwestward across the Pacific. Alaska is visible in the lower right corner of the map.

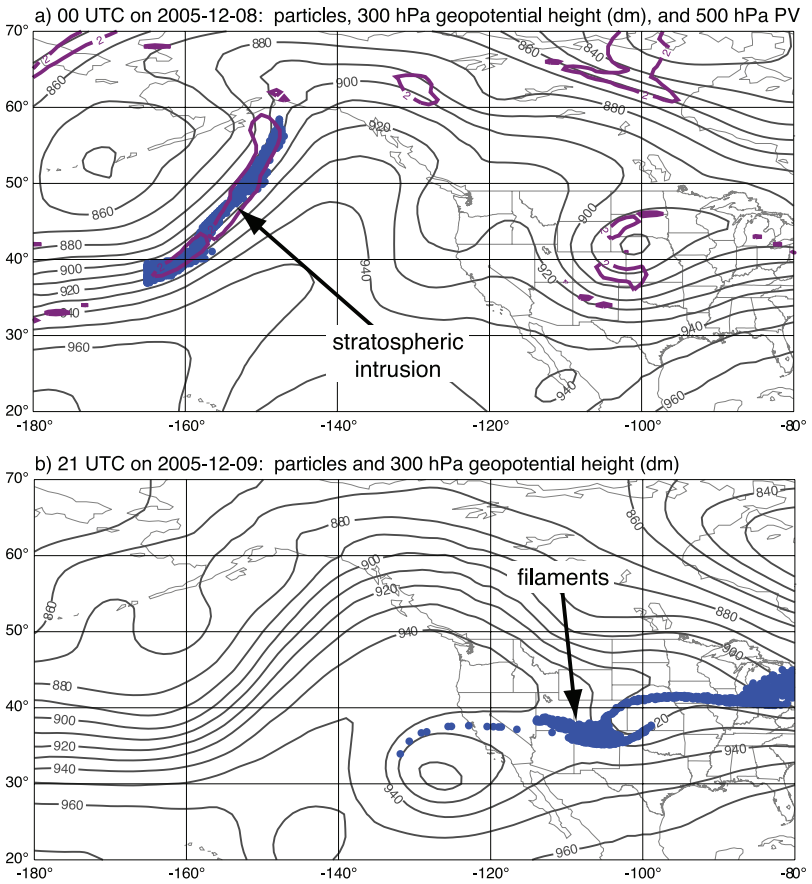

Figure 11. (a) Particle locations at 0000 UTC on 8 December 2005 (blue). Purple contours are 2 pvu isopleths at 500 hPa, indicating the location of the stratospheric intrusion in the jet stream over the Pacific Ocean. Gray contours are 300 hPa geopotential height. (b) Same particles at 2100 UTC on 9 December 2005. Particles satisfy the following criteria: in Figure 11a, $p > 300$ hPa and PV > 1.5 pvu, and in Figure 11b, pressures are near the aircraft flight level (275 to 325 hPa).

way agree very well with the high-resolution details of the water vapor image. In this case a substantial volume of air from widely separated sources was entrained into the low as it deepened. Unfortunately, the aircraft did not quite reach the boundary between these two air masses within the interior of the low, where we would have expected to observe a sharp gradient of moisture, and possibly ozone. Nevertheless, the results demonstrate clearly that it is possible to map the large-scale quasi-isentropic stirring in the atmosphere using only analyzed (or forecast) winds.

[33] Note that there are also two hyperbolic regions on either side of 110°W at about 45°N. These hyperbolic points are associated with a short wave in the main jet stream (Figure 2). The stretching method identifies these hyperbolic regions despite the fact that saddle points are not visible in the stream function.

5. Summary and Discussion

[34] Flight 5 of the HIAPER Progressive Science mission measured the chemical composition of the atmosphere in the region around a hyperbolic or saddle point in the upper tropospheric flow. This particular hyperbolic point was associated with a large cutoff low that formed off the west coast of North America (Figure 2). In good agreement with theory and with the calculated locations of the unstable manifolds, HIAPER observed a narrow filament of high-ozone, low-water-vapor air. The filament has a width of 50 km or less, which appears as two sharp spikes in the ozone concentration on the outbound and inbound legs of the flight track (Figure 7).

[35] Several different types of trajectory analysis were used to characterize the flow in the hyperbolic region and to identify the origin of the high-ozone air. The stretching analysis shows that the aircraft flew through three of the four quadrants surrounding the hyperbolic point. The flight track did not enter the southeastern quadrant. Typical trajectories for the two quadrants on the west side of the hyperbolic point can be seen in Figure 9. These trajectories show that air with very different recent histories, and by inference different chemical compositions, approaches the hyperbolic point from the north and south. The back trajectories also show that the high-ozone air in the two spikes lying along the unstable trajectories came from a stratospheric intrusion that occurred two to three days earlier in the main jet stream over the Pacific Ocean (Figures 10 and 11). That air, along with its acquired ozone, was stretched into a narrow filament by the flow near the hyperbolic point. Hyperbolic regions are primarily responsible for large-scale quasi-isentropic stirring, and this study

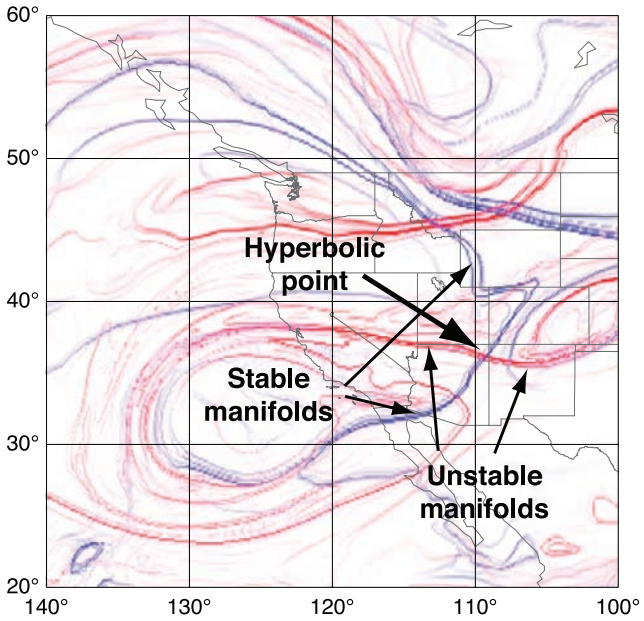

Figure 12. Stretching map at 320 K initialized at 1800 UTC on 9 December 2005. Trajectories were integrated for ±3 days. Red indicates large stretching for backward trajectories (unstable manifolds). Blue indicates large stretching for forward trajectories (stable manifolds). The hyperbolic point associated with the cutoff low is identified as the intersection of the red and blue curves near 109°W, 36°N.

demonstrates that they can be mapped in detail by finding the stable and unstable manifolds associated with the hyperbolic point using only knowledge of the large-scale winds (Figure 12).

[36] It is worth noting that the peak ozone value in the spikes is about 75 ppbv, which is well below typical stratospheric values, indicating that these parcels are mixtures of tropospheric and stratospheric air (Figure 8). With the available data it is not possible to say where the mixing occurred. It might have occurred as the stratospheric intrusion was forming, or after some amount of stratospheric air was entrained into the troposphere.

[37] From the results presented here, we conclude that, for Progressive Science flight 5, distinct small-scale features of the in situ chemical data can be clearly identified as resulting from transport by the large-scale flow. This includes both the stratospheric intrusion observed in the midtroposphere on the initial ascent and the fine structure observed near the hyperbolic point. Further stretching and thinning of the ozone filament as time goes on will rapidly reduce the width of the filament to the point that turbulence can mix it with the surrounding air. The 1° × 1° NCEP GFS analysis resolves the flow sufficiently well to represent the transport processes in the vicinity of the hyperbolic point and even captures the stratospheric intrusion relatively well. The kinematic analysis can be done as a regular part of flight planning by using recent meteorological analyses for back trajectories and model forecast winds for forward trajectories. Flight 5 was successfully planned this way (http://csrp.tamu.edu/hiaper/sections/hiaper_20051209T18Z.html).

[38] **Acknowledgments.** The authors would like to thank the many people who made the START and the Progressive Science Mission possible. This includes the staff of the NCAR Research Aviation Facility, particularly J. Stith, W. A. Cooper, D. C. Rogers, J. Jensen, and the HIAPER flight crews. W. Randel and C. Davis helped with flight planning and scientific discussions. Comments by two anonymous reviewers substantially improved this paper. This material is based upon work supported by the National Science Foundation under grant 0605739.

References

Appenzeller, C., and H. C. Davies (1992), Structure of stratospheric intrusions into the troposphere, *Nature*, *358*, 570–572.

Appenzeller, C., H. C. Davies, and W. A. Norton (1996), Fragmentation of stratospheric intrusions, *J. Geophys. Res.*, *101*, 1435–1456.

Beuermann, J., P. Konopka, D. Brunner, O. Bujok, G. Gunter, D. S. McKenna, J. Lilieveld, R. Muller, and C. Schiller (2002), High-resolution measurements and simulation of stratospheric and tropospheric intrusions in the vicinity of the polar jet stream, *Geophys. Res. Lett.*, *29*(12), 1577, doi:10.1029/2001GL014162.

Bowman, K. P. (1993), Large-scale isentropic mixing properties of the Antarctic polar vortex from analyzed winds, *J. Geophys. Res.*, *98*, 23,013–23,027.

Bowman, K. P., and G. D. Carrie (2002), The mean-meridional transport circulation of the troposphere in an idealized GCM, *J. Atmos. Sci.*, *59*, 1502–1514.

Haller, G. (2000), Finding finite-time invariant manifolds in two-dimensional velocity fields, *Chaos*, *10*, 99–108.

Haller, G., and A. C. Poje (1998), Finite time transport in aperiodic flows, *Physica D*, *119*, 352–380.

Miller, P., C. K. R. T. Jones, A. Rogerson, and L. Pratt, (1997), Quantifying transport in numerically generated velocity fields, *Physica D*, *110*, 105–122.

Ottino, J. M. (1989), *The Kinematics of Mixing: Stretching, Chaos, and Transport*, 364 pp., Cambridge Univ. Press, Cambridge, U. K.

Pan, L. L., et al. (2007), Chemical behavior of the tropopause observed during the Stratosphere-Troposphere Analyses of Regional Transport experiment, *J. Geophys. Res.*, *112*, D18110, doi:10.1029/2007JD008645.

Proffitt, M. H., and R. L. McLaughlin (1983), Fast-response dual-beam UV-absorption ozone photometer suitable for use on stratospheric balloons, *Rev. Sci. Instrum.*, *54*, 1719–1728.

Rogerson, A., P. Miller, L. Pratt, and C. K. R. T. Jones (1999), Lagrangian motion and fluid exchange in a barotropic meandering jet, *J. Phys. Oceanogr.*, *29*, 2635–2655.

Wiggins, S. (1992), *Chaotic Transport in Dynamical Systems*, 301 pp., Springer, New York.

Winkler, S. (2001), Lagrangian dynamics in geophysical fluid flows, Ph.D. thesis, 197 pp., Brown Univ., Providence, R. I.

Young, L.-H., et al. (2007), Enhanced new particle formation observed in the northern midlatitude tropopause region, *J. Geophys. Res.*, *112*, D10218, doi:10.1029/2006JD008109.

Yuan, G.-C., L. J. Pratt, and C. K. R. T. Jones (2002), Barrier destruction and Lagrangian predictability at depth in a meandering jet, *Dyn. Atmos. Oceans*, *35*, 41–61.

Yuan, G.-C., L. J. Pratt, and C. K. R. T. Jones (2004), Cross-jet Lagrangian transport and mixing in a $2\frac{1}{2}$-layer model, *J. Phys. Oceanogr.*, *34*, 1991–2005.

K. P. Bowman, Department of Atmospheric Sciences, Texas A&M University, 3150 TAMU, College Station, TX 77843-3150, USA. (k-bowman@tamu.edu)

T. Campos and L. L. Pan, National Center for Atmospheric Research, Boulder, CO 80307, USA.

R. Gao, Chemical Sciences Division, Earth System Research Laboratory, NOAA, Boulder, CO 80305, USA.